Current Applied Physics 16 (2016) 397–403

Contents lists available at ScienceDirect

Current Applied Physics

journal homepage: www.elsevier.com/locate/cap

Surface plasmonic effects on dye-sensitized solar cells by SiO_2-encapsulated Ag nanoparticles

Md Ashraf Hossain [a, 1], Jieun Park [b, 1], Dayoung Yoo [a, 1], Youn-kyoung Baek [c], Yangdo Kim [d], Soo Hyung Kim [a, e], Dongyun Lee [a, e, *]

[a] Department of Nano Fusion Technology, Pusan National University, Busan 609-735, Republic of Korea
[b] Department of Cogno-Mechatronics Engineering, Pusan National University, Busan 609-735, Republic of Korea
[c] Powder & Ceramics Division, Korea Institute of Materials Science, Changwon 642-831, Republic of Korea
[d] School of Materials Science and Engineering, Pusan National University, Busan 609-735, Republic of Korea
[e] Department of Nanoenergy Engineering, Pusan National University, Busan 609-735, Republic of Korea

ARTICLE INFO

Article history:
Received 20 December 2015
Received in revised form
5 January 2016
Accepted 6 January 2016
Available online 8 January 2016

Keywords:
Dye-sensitized solar cell
Surface plasmon resonance
Core–shell structure
$Ag@SiO_2$

ABSTRACT

A series of dye-sensitized solar cells (DSSCs) with different amounts of silver nanoparticles (Ag NPs) coated with a SiO_2 layer were prepared as core–shell $Ag@SiO_2$ nanoparticles ($Ag@SiO_2$ NPs). The influence of the amount of $Ag@SiO_2$ NPs on the performance of the DSSCs was investigated. As the amount of $Ag@SiO_2$ NPs increased, the intensity of the light-absorption spectra of the photoanodes gradually increased, whereas the amount of dye absorption was decreased. The short-circuit current density (J_{sc}), open-circuit voltage (V_{oc}), and power conversion efficiency (PCE) initially increased gradually and then decreased with increasing amounts of $Ag@SiO_2$ NPs; the charge-transfer resistance (R_2) exhibited the opposite trend. Optimal J_{sc}, V_{oc}, and PCE values of 13.85 mA/cm^2, 0.66 V, and 6.16%, respectively, were obtained in a DSSC containing 3 wt.% $Ag@SiO_2$ NPs; this PCE is 43.25% higher than that of a photoanode without $Ag@SiO_2$ NPs. The significant improvements in the properties of the optimal DSSC are attributed to the increase in the light coupling, which increased the light absorption of the dye, owing to the localized surface plasmon resonance of the $Ag@SiO_2$ NPs.

1. Introduction

Owing to the low cost of the component materials for the synthesis of the cells as well as the simple, cost-effective fabrication process [1,2], dye sensitized solar cell (DSSC) technology has attracted significant attention since DSSCs were introduced in 1991 [3]. DSSCs are typically sandwich-structured and composed of TiO_2 nanoparticles films covered with a monolayer of dye molecules as a photoanode, a redox electrolyte, and a counter electrode. To increase the efficiency of DSSCs by improving the photocurrent, photovoltage, or both, many studies have been focused on the photoanode, for which various types of TiO_2 morphologies have been extensively explored. These morphologies include nanoparticles (NPs) [4,5], ordered mesostructures [6], one-dimensional structures (nanorods, nanowires, and nanotubes) [7–10], and so on. In addition, the dye plays an important role in absorbing light, generating photo stimulated carriers, and injecting these carriers into the conduction band of the TiO_2 network. These phenomena affect the performance of the DSSCs. Therefore, increasing the light-absorption rate of the dye should increase the conversion efficiency.

The surface plasmon resonance (SPR) phenomenon is an interesting characteristic of novel metal NPs. SPR is generated between the electric fields of electromagnetic waves and free electrons in metal NPs. This phenomenon has been exploited for surface-enhanced spectroscopy [11], biological and chemical imaging [12,13], lithographic fabrication [14], and other applications [15,16]. SPR can enhance the apparent extinction coefficient of molecules adsorbed on suitable metal NPs [2,17]. Owing to their unique electronic, optical, and magnetic properties, the SPR of NPs of noble metals such as gold, silver, and copper has been recently used for DSSCs [18–20]. Silver (Ag) is a reasonably stable transition metal under ambient conditions. Nevertheless, it is easily corroded when

* Corresponding author. Department of Nanoenergy Engineering, Pusan National University, Busan 609-735, Republic of Korea.
E-mail address: dlee@pusan.ac.kr (D. Lee).
[1] Authors equally contributed.

http://dx.doi.org/10.1016/j.cap.2016.01.002
1567-1739/

it contacts acids or strong oxidants. Because electrolytes can permeate a porous TiO_2 film, bare Ag NPs dispersed in the film may be easily corroded by the electrolyte. This can undermine or even eliminate the SPR effect. Standridge et al. reported that in the case of photoelectrodes protected from corrosion, ~10 times more N3 (i.e., Ru(4,4′-carboxylic acid-2,2′-bipyridine)$_2$(NCS)$_2$) was adsorbed on nanosized Ag islands than on a bare fluorine-doped tin oxide (FTO) platform. This enhancement yielded a sevenfold increase in the overall energy-conversion efficiency [2]. Qi et al. investigated the effect of the SPR due to Ag NPs on the increase in the absorption of dye molecules; this study prompted a decrease in the thickness of photoanodes and hence an increase in the electron collection and device performance [21]. Furthermore, Jeong reported that the SPR of Ag NPs that are photo chemically incorporated into an electrode-supported TiO_2 nanoparticulate framework enhances the extinction of a subsequently adsorbed dye (the ruthenium-containing molecule, N719) [22]. Gangshetty et al. synthesized core–shell NPs comprising a triangular nanoprism core and a silica shell of variable thickness. This nanoprism silver particles exhibit a board SPR band centered at ~730 nm, which is overlaps well with the edge of the N719 absorption spectrum. They found that the incorporation of nanoprism silver particles into the photoanode of a DSSCs yielded a 32% increase in the overall power conversion efficiency (PCE) of the device [23]. However, the influence of Ag NPs and the mechanism governing their effect on the performance of DSSCs has scarcely been studied.

Thus, we fabricated monodisperse spherical Ag NPs encapsulated within a silica shell, Ag@SiO_2 NPs, and used them to improve the performance of DSSCs. Different amounts of core–shell-structured Ag@SiO_2 NPs were incorporated into TiO_2 nanocrystalline films in order to form composite photoanodes for the DSSCs, as schematically shown in Fig. 1. The influence of the Ag@SiO_2 NPs on the performance of the DSSCs, as well as the underlying mechanisms, was investigated.

2. Experimental procedure

2.1. Preparation of Ag core NPs

A 10-mL aqueous solution of 0.1 M silver nitrate ($AgNO_3$, Sigma Aldrich, USA) was stirred with a magnetic bar at elevated temperatures into a solution containing 100 mL of absolute ethanol (Sigma Aldrich, USA) and 50 mL of deionized (DI) water. Within 5 min, 20 mL of a 1 mM polyvinylpyrrolidone (Sigma Aldrich, USA) aqueous solution was added to the resulting mixture, which was stirred for 20 min. Next, 5.0 mL of 0.1 M sodium hydroxide (Junsei, Japan) was added to the solution, which was then cooled to room temperature. Ag NPs were obtained after a 2-h reaction.

2.2. Preparation of the Ag@SiO_2 NPs

The Ag@SiO_2 NPs solution was synthesized as follows. A mixture containing 50 mL of absolute ethanol (Sigma Aldrich, USA), 5.0 mL of ammonia (Junsei, Japan) and 1.0 mL of TEOS (Tetraethyl orthosilicate) (Sigma Aldrich, USA) was slowly added to the aforementioned silver colloids. The resulting solution was stirred at the ambient temperature for 12 h. The as-prepared product was washed with ethanol three times and then dispersed in ethanol for further use.

2.3. Fabrication of DSSC

For this experiment, TiO_2 paste was fabricated using commercially available TiO_2 NP powder (Titanium (IV) oxide, Sigma Aldrich, USA) without any subsequent treatment. In preparation for the screen-printing process, 0.3 g of TiO_2 NPs, 0.75 g of absolute ethanol (Sigma Aldrich, USA), 0.05 mL of acetic acid (CH_3COOH, Sigma Aldrich, USA), and 1 g of terpineol (Sigma Aldrich, USA) were mixed in a vial and sonicated for 1 h. In a different vial, 0.15 g of ethyl cellulose (Sigma Aldrich, USA) was dissolved in 1.35 g of ethanol. These two solutions were then homogeneously mixed for 1 h by using a sonicator. In the final step, the Ag@SiO_2 NPs solution was added to the TiO_2 paste solution in ratios ranging from 1% to 5%(w/w), and the resulting solution was homogeneously mixed by sonication for 1 h. The paste was then heated at 80 °C to evaporate the solvents; the color of the paste deepened as the amount of Ag@SiO_2 NPs increased. Prior to the fabrication of the Ag@SiO_2 NPs-containing TiO_2 NP photoelectrode films, an FTO-coated glass (2 cm × 2 cm, 7 Ω/sq, Solaronix, Switzerland) was cleaned by ultrasonication for 15 min in acetone, ethanol, and water, respectively. The FTO glass was dried by flowing nitrogen gas, immersed in a solution comprising $TiOCl_2$ (0.247 mL) and DI water (20 mL), and maintained at 70 °C [24]. It was then thermally treated at 350 and 500 °C for 30 min in order to form a buffer layer of anatase TPs,

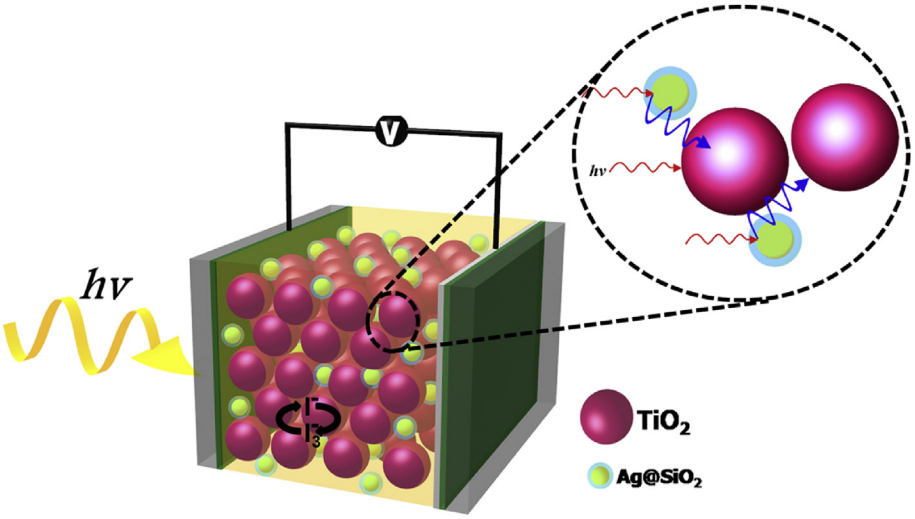

Fig. 1. A schematic showing the structure of a DSSC with a core–shell-structured Ag@SiO_2-incorporated TiO_2 films.

which acted as an adhesion layer for the subsequent TP layers. The TPs also inhibited the recombination of electron-hole pairs between the FTO and the electrolyte. A screen-printing method was then used to coat the prepared Ag@SiO_2 NPs-containing TiO_2 NPs onto the FTO glass. TiO_2 NP electrodes were prepared separately for comparison. After being dried in air, the TiO_2 NP and Ag@SiO_2 NPs-containing TiO_2 NP electrodes were sintered by the following process. First, the films were annealed for 10 min at 350 °C and for an additional 30 min at 500 °C [24]in a programmed tube furnace to remove the residual chemical constituents. After that, they were immersed in a dye solution (0.3 mM *of* N719 in 1:1 acetonitrile and tert-butanol) at room temperature for 24 h. The dye-soaked Ag@SiO_2 NPs-containing TiO_2 NP photoelectrode was rinsed with ethanol to remove the non-adsorbed dye and dried for 10 min in a convection oven at 80 °C.

The counter electrodes were placed on Pt-coated FTO glass, and a 0.4-mm-diameter hole was drilled in each FTO glass sample. A 5 mM solution of H_2PtCl_6 (Sigma Aldrich, USA) in ethanol was then drop-cast on the FTO glass and allowed to dry. The counter electrodes were calcined at 380 °C for 30 min. The dye-adsorbed TiO_2 NP photoelectrode and the Pt-coated counter electrode were assembled and bound with a hot-melt polymer film (60-μm-thick, Solaronix, Switzerland) that served as a spacer and defined the perimeter of the photo electrochemical sealing. These components were then placed in a convection oven at 120 °C and permanently combined by allowing the spacer to melt slightly. An iodide-based electrolyte solution (AN-50, Solaronix, Switzerland) was injected into the drilled hole on the back side of the platinized counter electrode, and the photocurrent conversion efficiency of the DSSC unit was immediately measured.

A 0.36 cm^2 (0.6 cm × 0.6 cm) active area of the resulting cell was exposed to light. Fig. 1 shows a schematic of the Ag@SiO_2 NPs-containing TiO_2 NP DSSC. The morphology of the samples was examined by scanning electron microscopy (Zeiss FE-SEM SUPRA25 and Raith Quantum Elphy). The photovoltaic properties of the DSSC were characterized using a solar simulator (PEC-L12, Pecell Technologies Inc.) under AM 1.5 and 1-sun (=100 mW/cm^2) illumination. The intensity of the sunlight illumination was calibrated using a standard Si photodiode. In addition, the electrochemical impedance spectra (EIS) were measured over the frequency range 0.5–10^5 Hz by applying a bias to the open-circuit voltage under an illumination of 100 mW/cm^2. The amount of dye loaded in the photoanodes was determined according to the ultraviolet–visible (UV–vis) spectra of the dye desorbed from these photoanodes upon their immersion in a solution containing water, ethanol (volume ratio = 1:1), and 0.1 M NaOH.

3. Results and discussion

Core–shell-structured SiO_2-encapsulated Ag NPs were used to enhance the PCEs of the DSSCs by SPR effects. The insulating SiO_2 shell acted as a barrier to prevent the electrical charging of the metal (Ag) core, thereby functioning as a propagating medium of the surface plasmon, specifically localized surface plasmonic resonating phenomenon (LSPR). As such, the SiO_2 shell was used (1) to create an electrically insulating layer between the Ag particles; (2) to prevent direct contact between the Ag NPs and the electrolyte, thereby inhibiting corrosion; (3) to separate Ag NPs and dye chromophores for effective LSPR [25]; and (4) to give the Ag NPs thermal and structural stability, thereby enabling thermal processing during device fabrication. It is also known that the shell could effectively prevent Oswald ripening.

Fig. 2(a) and (b) show SEM and TEM images, respectively, of Ag@SiO_2 NPs dispersed in an ethanol solution. The ~10-nm-large Ag spheres are encapsulated by the SiO_2 shell (see Fig. 2(b)). The

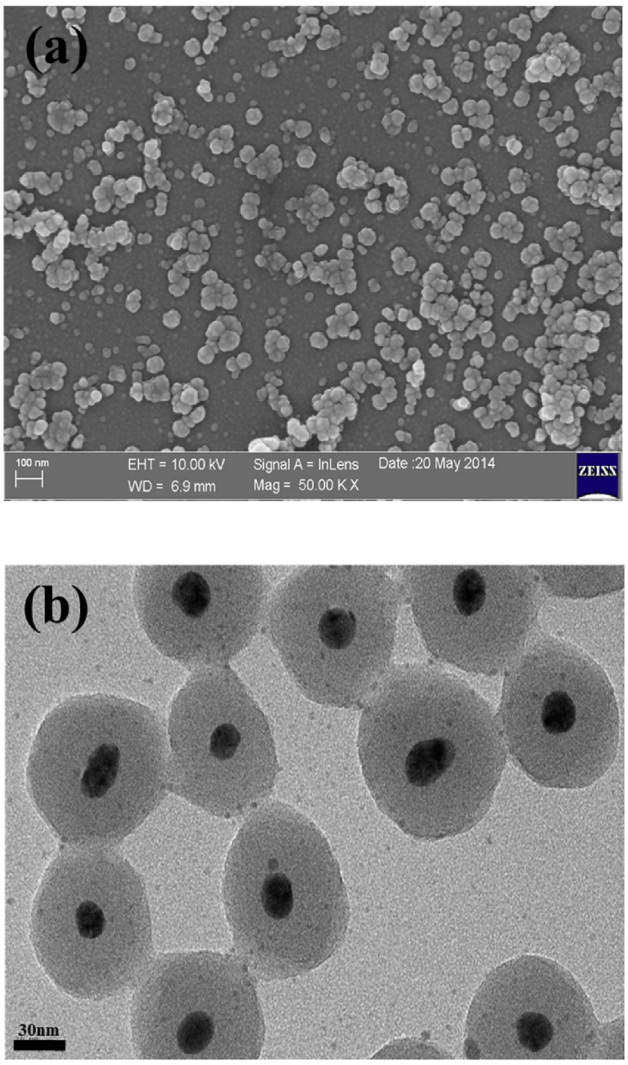

Fig. 2. Electron micrographs of the Ag@SiO_2 NPs: (a) SEM image of synthesized Ag with SiO_2 shells; (b) TEM image of Ag@SiO_2 NPs.

HRTEM image of Ag@SiO_2 NPs, shown in the inset of Fig. 2(b), reveals the clear lattice fringes, which are typical of crystalline Ag. Additionally, the corresponding UV–vis absorption spectra shown in Fig. 3(a) reveal that the absorption wavelength was slightly redshifted from 417 to 431 nm and the absorbance was significantly reduced when the particles were coated with SiO_2. The SiO_2 layer is considered to have reflected the incident light. To identify the effect of the SPR of Ag@SiO_2 NPs on the light absorption of the dye, mesoporous TiO_2 films with different amounts of incorporated Ag@SiO_2 NPs were prepared by the screen-printing method. To evaluate the contribution of Ag@SiO_2 NPs on the light-harvesting effect, the absorption spectra of the dye-absent and dye-desorbed photoanode films were measured, and the results are shown in Fig. 3(b) and (c). Fig. 3(b) shows the absorption spectra of the dye-absent films. Enhanced absorption of the TiO_2 films with Ag@SiO_2 was observed in the whole visible region of the spectra contrast to that of the pure TiO_2 pure film. We stated that the larger the content of Ag@SiO_2 in the system, the stronger the absorption of the visible light. An SPR band is observed in different films with Ag@SiO_2 NPs, which indicates that thermos stability of the treated Ag@SiO_2 NPs is acceptable. The UV–vis absorption spectra of the dye desorbed from the TiO_2 films, as measured in the NaOH

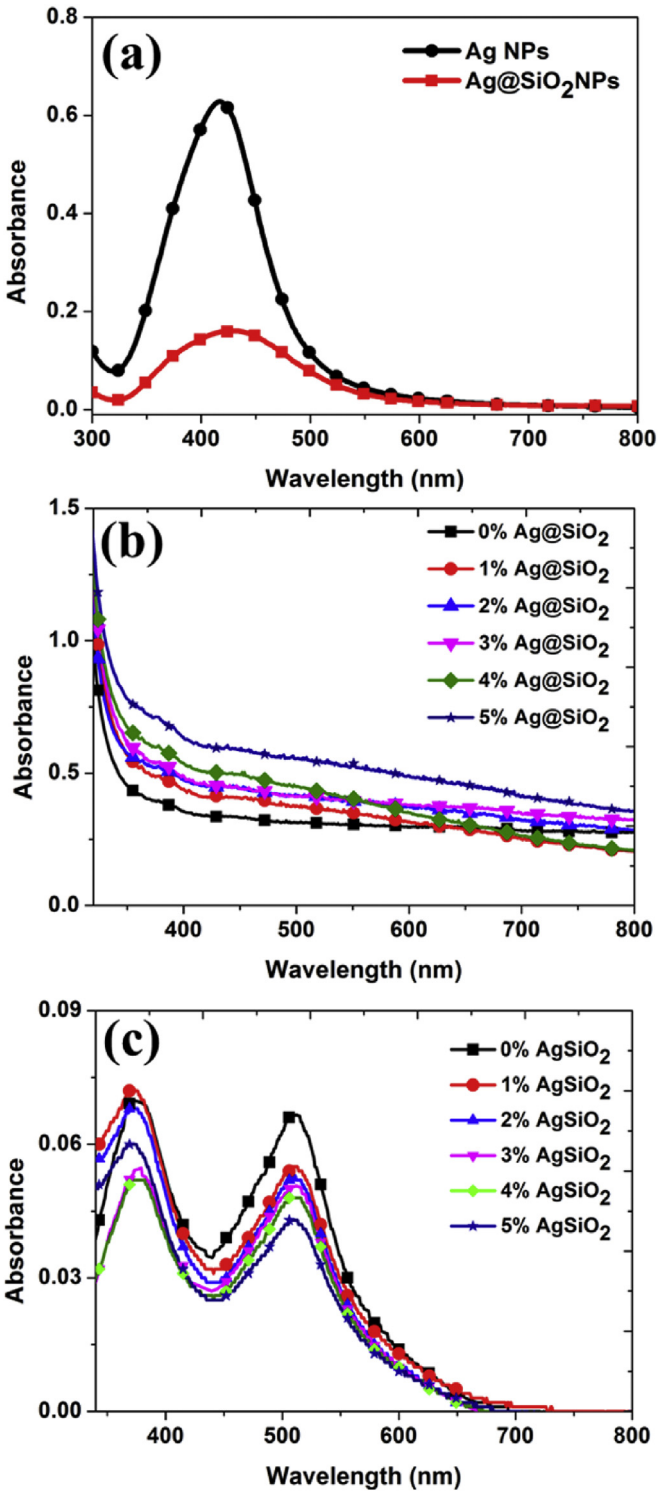

Fig. 3. UV–vis absorption spectra of; (a) Ag NPs before and after SiO_2coating; (b) absorption spectra of the TiO_2 films with different amounts of Ag@SiO_2 before dye loading; (c) absorption spectra of the dye desorbed from the TiO_2 films with different amounts of Ag@SiO_2 NPs.

solution, are shown in Fig. 3(c). The decrease in the absorbance of the Ag@SiO_2 NPs-containing films at 512 nm compared with the pure TiO_2 film indicates that less dye is loaded in the former than in the latter. This decrease in the amount of absorbed dye may stem from the reduction in the surface area of the TiO_2 films due to the incorporation of Ag@SiO_2 NPs. As we show later, the Ag@SiO_2 NPs-incorporated TiO_2 films exhibited a stronger light absorption than the pure TiO_2 film, despite having a lower dye-loading capacity.

A series of DSSCs composed of N719-dye-sensitized TiO_2-film photoanodes with varying amounts of Ag@SiO_2 NPs were prepared in order to determine the effect of the addition of Ag@SiO_2 NPs on their performance. The cell employed as the DSSC is shown in Fig. 4(a). Fig. 4(b) shows an SEM image of the cell in plan and cross-sectional (inset) views; one is clearly noticed that the absorption layers were composed of TiO_2 nanoparticles and encapsulated Ag nanoparticles (see also Fig. 4(c)). The photocurrent density-voltage (*J-V*) characteristics of these DSSCs are shown in Fig. 5(a). As the *J-V* curves show, the short-circuit current density (J_{sc}) changed significantly and systematically with respect to the concentration of Ag@SiO_2 NPs; i.e., J_{sc} increased monotonically as the Ag@SiO_2 NPs content increased to 2 wt.%. At 3 wt.% of Ag@SiO_2 NPs, J_{sc} increased substantially to ~14 mA/cm^2, which is more than 35% higher than that for the pure TiO_2 film. J_{sc} decreased as the Ag@SiO_2 NPs content increased further. These results were directly influenced by the PCE of the cell. The parameters, which describe the cell performance, are presented in Table 1.

Table 1 shows that the amount of dye loaded in the films decreased gradually as the amount of Ag@SiO_2 NPs increased. However, the PCE of the cells increased as the Ag@SiO_2 NPs content increased to 3 wt.% and decreased thereafter. We attribute these phenomena to the SPR effect and light scatter effect of the core–-shell particles [26]. SPR effect of the composite stimulated by illumination light leads to the collective excitation oscillations and thus created a strong enhancement of the localized electromagnetic fields around the Ag@SiO_2 nanoparticles. By the enhanced electromagnetic field improving the interaction with the dye molecules dipoles, the enhanced light absorption of the dye and more charge carrier generation can be achieved [20,27]. As previously mentioned, less dye was loaded in the Ag@SiO_2 NPs doped TiO_2 films compared with the pure TiO_2 film. Therefore, the increase in J_{sc} is mainly attributed to the enhanced light absorption due to the interaction between its molecular dipoles and the enhanced electromagnetic field induced by the SPR of Ag@SiO_2 NPs. It is assumed that the SPR effect increases the coupling of light and the amount of photon energy transferred to the dye, increasing the generation of charge carriers [28]. The enhanced J_{sc} may also arise from the increased SPR-induced light scattering in the visible range of the Ag@SiO_2 NPs-containing composite films; this increased scattering increases the optical path, reduces the transmission of the incident light, and increases the likelihood of the dye molecules capturing the photons and converting them into charge carriers [21,29,30]. However, the J_{sc} decreased for Ag@SiO_2 NPs contents higher than 3 wt.%. This decrease for excess amounts of Ag@SiO_2 NPs was possibly due to a reduction in the effective surface area of the films and the amount of dye absorbed, as well as an increase in the charge-carrier recombination [31,32].

To confirm the origin of this improvement in the PCE, incident photon-to-electron conversion efficiency (IPCE) measurements were performed on several of the completed devices, and the results are shown in Fig. 5(b). Because the current density in a solar cell is governed by the integral of the product of the photon flux and the IPCE, any changes to the value of J_{sc} should be reflected in the IPCE spectra. The results agree well with the trends observed in the *J-V* curves. The DSSC with 3 wt.% Ag@SiO_2 NPs exhibited a notably higher IPCE than the 0 wt.% Ag@SiO_2 NPs photoanode.

Fig. 6 shows the dependence of the DSSC performance parameters—the photocurrent density (J_{sc}), open-circuit voltage (V_{oc}), fill factor (FF), and PCE—on the Ag@SiO_2 NPs content of the TiO_2 films. As shown previously, the J_{sc} increased monotonically as the Ag@SiO_2 NPs content increased to 3 wt.% and decreased thereafter.

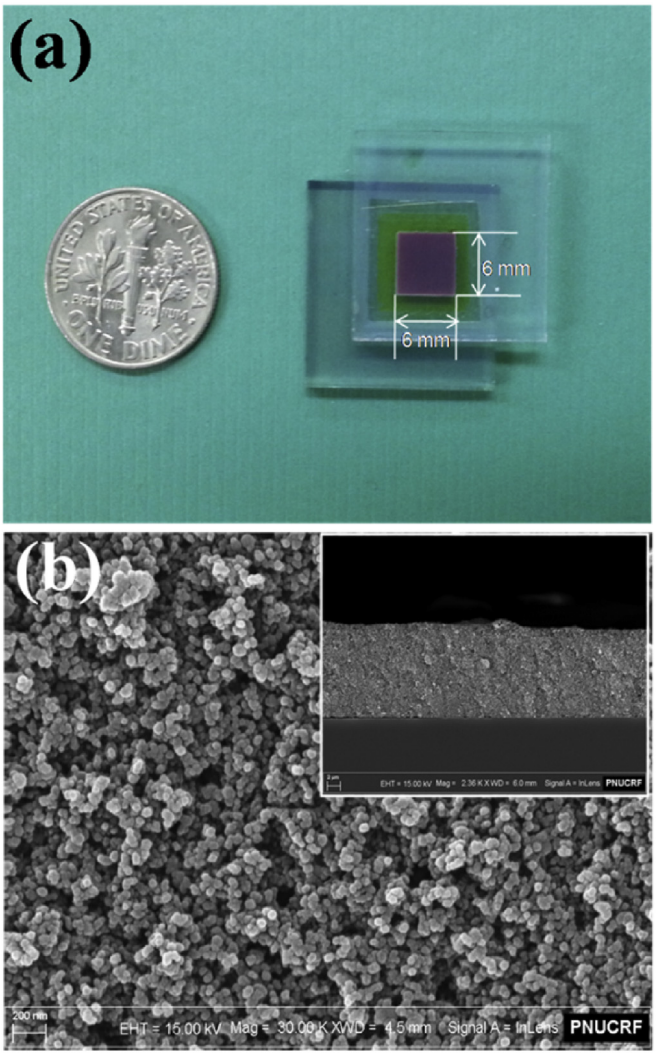

Fig. 4. Photograph of an assembled DSSC unit cell, (a); SEM images showing top and cross-sectional (inset) views of the photoanode with accumulated Ag@SiO_2 NPs-containing TiO_2 NPs, (b); X-ray diffraction (XRD) patterns of accumulated Ag@SiO_2 NPs-containing photoanode, (c).

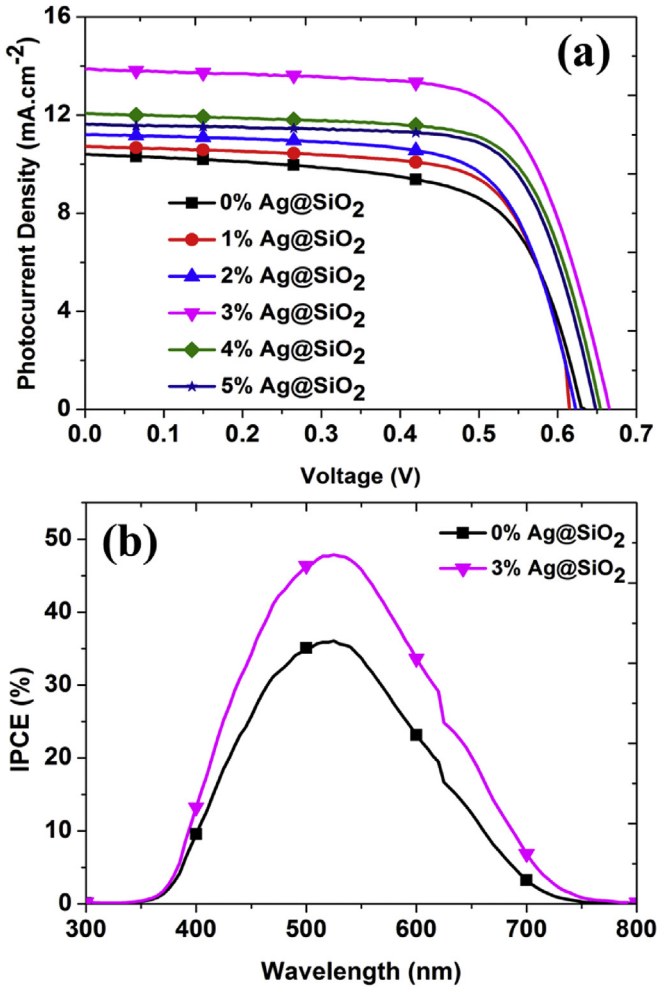

Fig. 5. *J-V* curves of DSSCs containing different amounts of Ag@SiO_2 NPs on photoanode, (a); and IPCE of DSSCs, (b).

The optimal J_{sc} of ~14 mA/cm^2 was obtained for the DSSC with a Ag@SiO_2 NPs content of 3 wt.%; this optimal J_{sc} is more than 35% higher than that (10.20 mA/cm^2) of the DSSC comprising a pure TiO_2 photoanode. Moreover, the PCE exhibits a similar dependence on the Ag@SiO_2 NPs content; i.e., the maximum PCE (6.16%), which is 43.25% higher than that (4.30%) of the conventional DSSC, is obtained in the case of the 3 wt.% Ag@SiO_2 NPs-containing DSSC. These results suggest that the significantly enhanced J_{sc} and PCE of the Ag@SiO_2 NPs-containing DSSC result from the SPR of Ag@SiO_2 NPs. We observed the increase of V_{oc}, which is normally limited by the electronic structures of the materials. The improved V_{oc} arises from the electron-storage capability of Ag@SiO_2 NPs. The rapid transfer of electrons from the conduction band of TiO_2 NPs to Ag@SiO_2 NPs and their subsequent storage yield the improved photo electrochemical performance of the Ag@SiO_2–TiO_2 films. This electron storage shifts the quasi-Fermi energy of the Ag–TiO_2 composite system to a more negative level compared with that of the pure TiO_2 photoanode, yielding a V_{oc} higher than that of the pure TiO_2 photoanode, as exhibited by the DSSC containing 3 wt.% Ag@SiO_2 NPs (Table 1 and Fig. 6(b)) [33]. Compared with those of conventional DSSCs, the FFs of the Ag@SiO_2 NPs-containing DSSC (Table 1 and Fig. 6(b)) exhibit no obvious tendencies.

EIS of DSSCs is typically performed to reveal the differences in the charge-transfer resistance at the conducting layer/TiO_2, Pt/electrolyte, and dye/TiO_2/electrolyte interfaces [34]. We drew EIS Nyquist plots of the DSSCs with and without Ag@SiO_2 NPs at the same forward bias, and typical examples are shown in Fig. 7(a). In

Table 1
Photovoltaic-characterization results of DSSCs based on different photoanodes[a].

Sample	J_{sc}(mA cm^{-2})	V_{oc}(V)	FF	PCE(%)	R_2(Ω)	M_{DA} (×10^{-7} mol cm^{-2})
0 wt.% Ag@SiO_2	10.20	0.63	0.67	4.30	10.4	1.57
1 wt.% Ag@SiO_2	10.61	0.62	0.70	4.60	7.72	1.29
2 wt.% Ag@SiO_2	11.11	0.62	0.69	4.75	7.88	1.22
3 wt.% Ag@SiO_2	13.85	0.66	0.67	6.16	6.64	1.19
4 wt.% Ag@SiO_2	12.00	0.65	0.69	5.44	7.18	1.13
5 wt.% Ag@SiO_2	11.62	0.65	0.70	5.27	7.82	1.01

[a] J_{sc} = short-circuit current density, V_{oc} = open-circuit voltage, FF = fill factor, PCE = power conversion efficiency, M_{DA} = amount of dye absorbed.

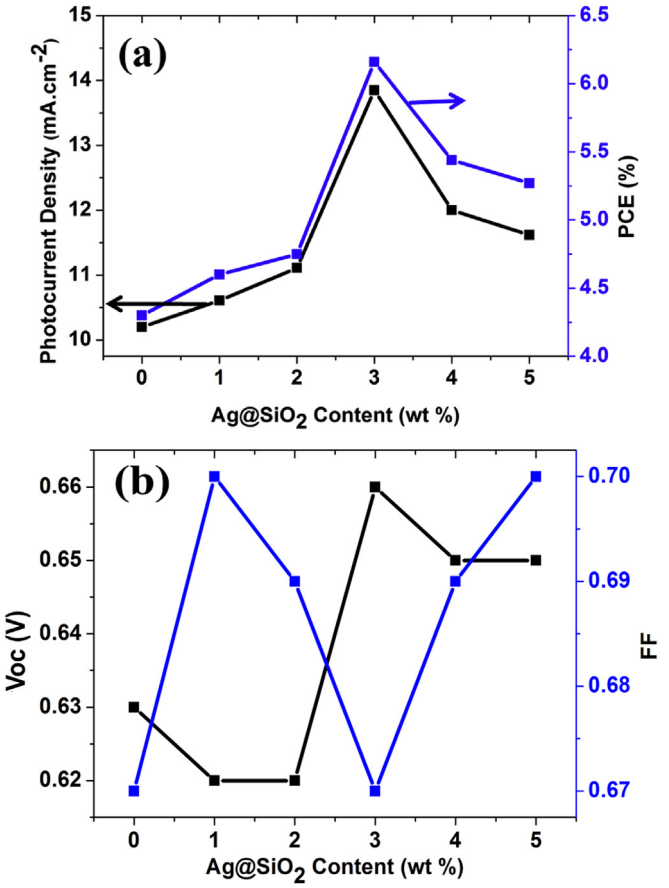

Fig. 6. Variation in the DSSC parameters with respect to the contents of Ag@SiO_2 NPs: (a) J_{sc} and overall PCE; (b) V_{oc} and Fill Factor.

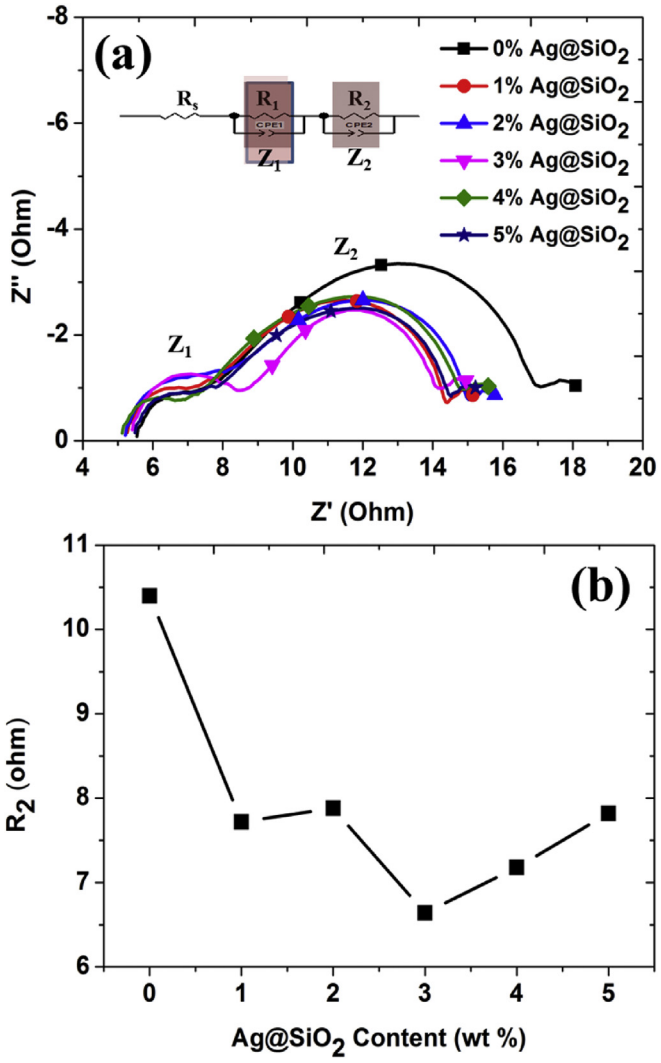

Fig. 7. Nyquist plots obtained from the EIS of DSSCs with varying Ag@SiO_2 content (inset shows the equivalent circuit), (a); and R_2 with respect to the Ag@SiO_2 NPs content, (b).

the equivalent circuit, Z_1 represents the complex impedance of the charge transfer at the TiO_2 conduction layer or Pt/electrolyte interface, and Z_2 is the complex impedance of the TiO_2/dye/electrolyte interface [35]. Because the same Pt-coated counter-electrode is applied in each of the DSSCs, the influence of Z_1 can be ignored. Our interest in the EIS spectra lies mainly in the charge-transfer resistance R_2 (real part of Z_2), which is associated with the electron transfer at the TiO_2/dye/electrolyte interface. As Fig. 7(a) shows, the diameter of Z_2 decreased monotonically as the Ag@SiO_2 NPs content increased to 3 wt.%. Accordingly, R_2 (Fig. 7(b)), which was fitted using the simulation circuits (inset of Fig. 7(a)), decreased from 10.4 Ω for the conventional DSSC to 6.64 Ω for the 3 wt.%Ag@SiO_2 NPs-containing DSSC. Additionally, as shown in the Nyquist plots, the amount of recombination of electrons with triiodide ions and the excited dye at the TiO_2/dye/electrolyte interface [36] decreased as the diameter of Z_2 decreased. However, R_2 increased for Ag@SiO_2 NPs contents higher than 3 wt.%. This increase possibly arose from the excess Ag@SiO_2 NPs, which reduced the contact between the dye and the TiO_2N-Psandincreasedthe electron-transport length and, hence, the chance of recombination [32].

4. Conclusion

A series of composite TiO_2photoanodes with different amounts of Ag@SiO_2 NPs were prepared and used to fabricate various DSSCs. The influence of Ag@SiO_2 NPs on the performance of the

photoanodes and DSSCs was investigated. The results revealed that the introduction of Ag@SiO_2 NPscan enhance the light-absorption capacity of the photoanodes. Increasing the Ag@SiO_2 NPs content of the photoanodes caused a gradual increase and a monotonic decrease, respectively, in the intensity of the light-absorption spectra and the amount of dye absorbed. In addition, the J_{sc} and PCE increased gradually as the Ag@SiO_2 NPs content increased to 3 wt.% and decreased thereafter; however, the charge-transfer resistance R_2 exhibited the opposite trend, decreasing as the Ag@SiO_2 NPs content increased to 3 wt.% and increasing thereafter. Optimal J_{sc}, V_{oc}, and PCE values of 13.85 mA/cm^2, 0.66 V, and 6.16%, respectively, were obtained for a Ag@SiO_2 NPs content of 3 wt.%; the optimal PCE was 43.25% higher than that of a 0 wt.%-Ag@SiO_2 NPs photoanode. The significant improvements in the properties of the DSSC are attributed to the increased light absorption of the dye due to the increased light coupling caused by the SPR of Ag@SiO_2 NPs.

Acknowledgment

This research was co-supported by 1) the National Research Foundation of Korea (NRF) grant funded by the Korea government (MSIP) (No. 2015R1A2A2A01002795), and 2) the Civil & Military Technology Cooperation Program, through the National Research Foundation of Korea (NRF), funded by the Ministry of Science, ICT & Future Planning (No. 2013M3C1A9055407).

References

[1] M.K. Nazeeruddin, R. Humphry-Baker, P. Liska, M. Grätzel, Investigation of sensitizer adsorption and the influence of protons on current and voltage of a dye-sensitized nanocrystalline TiO_2 solar cell, J. Phys. Chem. B 107 (2003) 8981–8987.
[2] S.D. Standridge, G.C. Schatz, J.T. Hupp, Distance dependence of plasmon-enhanced photocurrent in dye-sensitized solar cells, J. Am. Chem. Soc. 131 (2009) 8407–8409.
[3] M. G, B. O'Regan, A low-cost high- efficiency solar cell based on dye sensitized colloidal TiO_2 films, Nature 353 (1991) 737–740.
[4] M. Grätzel, Dye-sensitized solar cells, J. Photochem. Photobiol.C 4 (2003) 145–153.
[5] T.H. Meen, W. Water, W.R. Chen, S.M. Chao, L.W. Ji, C.J. Huang, Application of TiO_2 nano-particles on the electrode of dye-sensitized solar cells, J. Phys. Chem. Solids 270 (2009) 472–476.
[6] L. Hu, S. Dai, J. Weng, S. Xiao, Y. Sui, Y. Huang, S. Chen, F. Kong, X. Pan, L. Liang, K. Wang, Microstructure design of nanoporous TiO_2 photoelectrodes for dye-sensitized solar cell modules, J. Phys. Chem. B 111 (2006) 358–362.
[7] X. Liu, M. Guo, J. Lin, X. Chen, H. Huang, Design of multi-layered TiO_2 nanotube/nanoparticle hybrid structure for enhanced efficiency in dye-sensitized solar cells, RSC Adv. 4 (2014) 45180–45184.
[8] X. Feng, K. Shankar, O.K. Varghese, M. Paulose, T.J. Latempa, C.A. Grimes, Vertically aligned single crystal TiO_2 nanowire arrays grown directly on transparent conducting oxide coated glass: synthesis details and applications, Nano Lett. 8 (2008) 3781–3786.
[9] M. Adachi, Y. Murata, J. Takao, J. Jiu, M. Sakamoto, F. Wang, Highly efficient dye-sensitized solar cells with a titania thin-film electrode composed of a network structure of single-crystal-like TiO_2 nanowires made by the "oriented attachment" mechanism, J. Am. Chem. Soc. 126 (2004) 14943–14949.
[10] G.K. Mor, K. Shankar, M. Paulose, O.K. Varghese, C.A. Grimes, Use of highly-ordered TiO_2 nanotube arrays in dye-sensitized solar cells, Nano Lett. 6 (2005) 215–218.
[11] S. Nie, S.R. Emory, Probing single molecules and single nanoparticles by surface-enhanced raman scattering, Science 275 (1997) 1102–1106.
[12] L.S. Jung, C.T. Campbell, T.M. Chinowsky, M.N. Mar, S.S. Yee, Quantitative interpretation of the response of surface plasmon resonance sensors to adsorbed films, Langmuir 14 (1998) 5636–5648.
[13] J.M. Brockman, B.P. Nelson, R.M. Corn, Surface plasmon resonance imaging measurements of ultrathin organic films, Annu. Rev. Phys. Chem. 51 (2000) 41–63.
[14] W. Srituravanich, N. Fang, C. Sun, Q. Luo, X. Zhang, Plasmonic nano-lithography, Nano Lett. 4 (2004) 1085–1088.
[15] K.A. Willets, R.P. Van Duyne, Localized surface plasmon resonance spectroscopy and sensing, Annu. Rev. Phys. Chem. 58 (2007) 267–297.
[16] K.L. Kelly, E. Coronado, L.L. Zhao, G.C. Schatz, The optical properties of metal nanoparticles: the influence of size, shape, and dielectric environment, J. Phys. Chem. B 107 (2002) 668–677.
[17] M. Ihara, K. Tanaka, K. Sakaki, I. Honma, K. Yamada, Enhancement of the absorption coefficient of cis-(NCS)2 Bis(2,2′-bipyridyl-4,4′-dicarboxylate) ruthenium(II) dye in dye-sensitized solar cells by a silver island film, Annu. Rev. Phys. Chem. 101 (1997) 5153–5157.
[18] S.P. Lim, A. Pandikumar, N.M. Huang, H.N. Lim, G. Gu, T.L. Ma, Promotional effect of silver nanoparticles on the performance of N-doped TiO_2 photoanode-based dye-sensitized solar cells, RSC Adv. 4 (2014) 48236–48244.
[19] O. Amiri, M. Salavati-Niasari, A. Rafiei, M. Farangi, 147% improved efficiency of dye synthesized solar cells by using CdS QDs, Au nanorods and Au nanoparticles, RSC Adv. 4 (2014) 62356–62361.
[20] H. Dong, Z. Wu, Y. Gao, A. El-Shafei, S. Ning, J. Xi, B. Jiao, X. Hou, Silver-loaded anatase nanotubes dispersed plasmonic composite photoanode for dye-sensitized solar cells, Org. Electron 15 (2014) 2847–2854.
[21] J. Qi, X. Dang, P.T. Hammond, A.M. Belcher, Highly efficient plasmon-enhanced dye-sensitized solar cells through metal@oxide core–shell nanostructure, ACS Nano 5 (2011) 7108–7116.
[22] N.C. Jeong, C. Prasittichai, J.T. Hupp, Photocurrent enhancement by surface plasmon resonance of silver nanoparticles in highly porous dye-sensitized solar cells, Langmuir 27 (2011) 14609–14614.
[23] M.K. Gangishetty, K.E. Lee, R.W.J. Scott, T.L. Kelly, Plasmonic enhancement of dye sensitized solar cells in the red-to-near-infrared region using triangular core–shell Ag@SiO_2 nanoparticles, ACS Appl. Mater. Interfaces 5 (2013) 11044–11051.
[24] J.Y. Ahn, J.H. Kim, K.J. Moon, S.D. Park, S.H. Kim, Synergistic effects of the aspect ratio of TiO_2 nanowires and multi-walled carbon nanotube embedment for enhancing photovoltaic performance of dye-sensitized solar cells, Nanoscale 5 (2013) 6842–6850.
[25] N. Liu, B.S. Prall, V.I. Klimov, Hybrid gold/silica/nanocrystal-quantum-dot superstructures: synthesis and analysis of semiconductor–metal interactions, J. Am. Chem. Soc. 128 (2006) 15362–15363.
[26] Z. Tian, L. Wang, L. Jia, Q. Li, Q. Song, S. Su, H. Yang, A novel biomass coated Ag-TiO_2 composite as a photoanode for enhanced photocurrent in dye-sensitized solar cells, RSC Adv. 3 (2013) 6369–6376.
[27] M.D. Brown, T. Suteewong, R.S.S. Kumar, V. D'Innocenzo, A. Petrozza, M.M. Lee, U. Wiesner, H.J. Snaith, Plasmonic dye-sensitized solar cells using core–shell metal–insulator nanoparticles, Nano Lett. 11 (2010) 438–445.
[28] C. Hägglund, M. Zäch, B. Kasemo, Enhanced charge carrier generation in dye sensitized solar cells by nanoparticle plasmons, Appl. Phys. Lett. 92 (2008) 013113.
[29] B. Ding, B.J. Lee, M. Yang, H.S. Jung, J.-K. Lee, Surface-plasmon assisted energy conversion in dye-sensitized solar cells, Adv. Energy Mater. 1 (2011) 415–421.
[30] D.D. Evanoff, G. Chumanov, Size-controlled synthesis of nanoparticles. 2. Measurement of extinction, scattering, and absorption cross sections, J. Phys. Chem. B 108 (2004) 13957–13962.
[31] M. Ihara, M. Kanno, S. Inoue, Photoabsorption-enhanced dye-sensitized solar cell by using localized surface plasmon of silver nanoparticles modified with polymer, Phys. E Low Dimens. Syst. Nanostruct. 42 (2010) 2867–2871.
[32] W. Hou, P. Pavaskar, Z. Liu, J. Theiss, M. Aykol, S.B. Cronin, Plasmon resonant enhancement of dye sensitized solar cells, Energy Environ. Sci. 4 (2011) 4650–4655.
[33] A. Takai, P.V. Kamat, Capture, store, and discharge. Shuttling photogenerated electrons across TiO2–Silver interface, ACS Nano 5 (2011) 7369–7376.
[34] Q. Wang, J.-E. Moser, M. Grätzel, Electrochemical impedance spectroscopic analysis of dye-sensitized solar cells, J. Phys. Chem. B 109 (2005) 14945–14953.
[35] L. Han, N. Koide, Y. Chiba, T. Mitate, Modeling of an equivalent circuit for dye-sensitized solar cells, Appl. Phys. Lett. 84 (2004) 2433–2435.
[36] C.-S. Chou, R.-Y. Yang, C.-K. Yeh, Y.-J. Lin, Preparation of TiO2/Nano-metal composite particles and their applications in dye-sensitized solar cells, Powder Technol. 194 (2009) 95–105.